Fixed Depth Hamiltonian Simulation via Cartan Decomposition

Efekan Kökcü,[1, *] Thomas Steckmann,[1] J. K. Freericks,[2] Eugene F. Dumitrescu,[3, †] and Alexander F. Kemper[1, ‡]

[1]*Department of Physics, North Carolina State University, Raleigh, North Carolina 27695, USA*
[2]*Department of Physics, Georgetown University, 37th and O Sts. NW, Washington, DC 20057 USA*
[3]*Computational Sciences and Engineering Division,*
Oak Ridge National Laboratory, Oak Ridge, TN 37831, USA
(Dated: May 5, 2021)

Simulating spin systems on classical computers is challenging for large systems due to the significant memory requirements. This makes Hamiltonian simulation by quantum computers a promising option due to the direct representation of quantum states in terms of its qubits. Standard algorithms for time evolution on quantum computers require circuits whose depth grows with time. We present a new algorithm, based on Cartan decomposition of the Lie algebra generated by the Hamiltonian, that generates a circuit with time complexity $\mathcal{O}(1)$ for ordered and disordered models of n spins. We highlight our algorithm for special classes of models where an $\mathcal{O}(n^2)$-gate circuit emerges. Compared to product formulas with significantly larger gate counts, our algorithm drastically improves simulation precision. Our algebraic technique sheds light on quantum algorithms and will reduce gate requirements for near term simulation.

Creating arbitrary unitary operations with a sequence of one and two-qubit gates is the central task for quantum compilation. This task of *unitary synthesis* broadly applies to quantum state preparation (e.g. via the unitary coupled cluster formalism), thermal state preparation (by a unitary embedding of a mixed state), and quantum arithmetic logic. In this realm, a paradigmatic problem [1, 2] is the unitary synthesis of time evolution under a time-independent Hamiltonian $\mathcal{H}$; *i.e.*, the unitary $U = e^{-i\mathcal{H}t}$. While the circuit complexity of an arbitrary unitary grows exponentially with the number of qubits, for Hamiltonian evolution a number of efficient, approximate decomposition techniques exist based on product formulas [3–5], series expansions [6], and other techniques [7–9]. These algorithms are optimized for sparse Hamiltonians, with circuit depth scaling almost linearly in the evolution time and inverse logarithmically in the approximation error.

Despite the efficient asymptotic performance the above algorithms, the exponential decay of the circuit fidelity with respect to circuit depth in the absence of error correction prevents useful Hamiltonian simulation in present hardware. Thus, even though polynomial time quantum algorithms for certain simulations are known, reducing the circuit depth required for simulations remains of interest to the field. Recent work to this end has begun to incorporate additional problem information such as algebraic properties, system symmetries [10], and initial states [11] to further improve Hamiltonian time-evolution.

Concurrent with the above synthesis techniques, an optimal unitary synthesis of arbitrary two-qubit operations based on the Cartan decomposition has emerged as the state-of-the-art technique [12]. For larger unitaries, Refs. 13 and 14 shows how any element in $SU(2^n)$ can be recursively decomposed, but even these methods generically require exponential circuit depth for arbitrary unitaries. The decomposition works as follows. Consider a time-independent Hamiltonian for n qubits (or n spin-½ particles)

$$\mathcal{H} = \sum_j H_j \sigma^j, \tag{1}$$

where H_j are coefficients and σ^j are Pauli string operators: *i.e.*, elements of the n-site Pauli group $\mathcal{P}_n = \{I, X, Y, Z\}^{\otimes n}$. Ref. 13 recursively obtains a factorization of the time-evolution unitary as

$$U(t) = e^{-i\mathcal{H}t} = \prod_{\bar{\sigma}^i \in \mathfrak{su}(2^n)} e^{i\kappa_i \bar{\sigma}^i}, \tag{2}$$

with, in the general case, $\mathcal{O}(4^n)$ angles κ_i for the Pauli strings $\bar{\sigma}^i$ that form a basis for the Lie algebra $\mathfrak{su}(2^n)$. However, this method has not found widespread application due to the exponential cost of representing the product in Eq. (2).

The challenge in directly implementing this approach raises the question: are there systems or other factorization algorithms for which the Cartan decomposition can emerge as an efficient technique with a broader application? In this work, we answer this question in the

affirmative by providing a Cartan-based decomposition algorithm that generates exact Hamiltonian simulation circuits whose depth is constant in time. In addition, the problem of finding the numerical parameters κ_i is reduced to locating a local, rather than global, minimum of a cost function that can be computed in polynomial time. To illustrate our algorithm, we apply it to the ubiquitous test case of spin models which are isomorphic to non-interacting fermion models [15]; in this case, the circuit complexity reduces to a polynomial in the system size. We use this circuit to time evolve a 10-site spin system and compare the result to a Trotter approach with equal or greater depth to illustrate the dramatic improvements obtained.

Hamiltonian Algebra—For a given Hamiltonian, we determine whether the entirety of $\mathfrak{su}(2^n)$ is necessary for the expansion in Eq. (2), or whether a subset suffices. The Baker-Campbell-Hausdorff theorem states that only nested commutators of the individual terms in the Hamiltonian appear in the final exponent. This leads us to the **first step of our algorithm:** Using the expansion of the Hamiltonian in terms of the Pauli terms σ^j in Eq. (1), find the closure (under commutation) of the set of those Pauli terms. This closure forms a basis for the *Hamiltonian algebra*, which we denote as $\mathfrak{g}(\mathcal{H})$, and which is a subalgebra of $\mathfrak{su}(2^n)$ [16]. We can now restrict the expansion in Eq. (2) to only the elements of $\mathfrak{g}(\mathcal{H})$, which notably are independent of the coefficients H_j.

Fig. 1 illustrates the dimension of the Hamiltonian algebra $|\mathfrak{g}(\mathcal{H})|$ for various models of interest as a function of system size n, where $|\cdot|$ denotes the dimension of the algebra. The dimensions of the Hamiltonian algebra for the n-site nearest-neighbor XY, transverse field XY (TFXY) and transverse field Ising (TFIM) models are $|\mathfrak{g}(\mathrm{XY})| =$
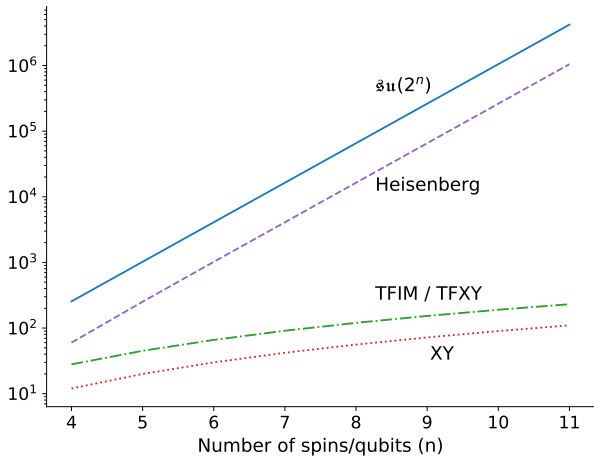
FIG. 1. Hamiltonian algebra dimension for the nearest-neighbor Heisenberg, XY, TFIM and TFXY models, and dimension of full $\mathfrak{su}(2^n)$ for comparison to the generic case. The dimensions can exactly be calculated as $|\mathfrak{g}(\mathrm{Heisenberg})| = 4^{n-1} - 4$, $\mathfrak{g}(|\mathrm{TFIM})| = |\mathfrak{g}(\mathrm{TFXY})| = n(2n-1)$ and $|\mathfrak{g}(\mathrm{XY})| = n(n-1)$.

$n(n-1)$ and $|\mathfrak{g}(\mathrm{TFIM})| = |\mathfrak{g}(\mathrm{TFXY})| = n(2n-1)$; these scale *quadratically* with the number of qubits n. On the other hand, $|\mathfrak{g}(\mathcal{H})|$ for the nearest-neighbor Heisenberg model scales exponentially, $|\mathfrak{g}(\mathrm{Heisenberg})| = 4^{n-1} - 4$. We observe a similar exponential growth in TFXY and TFIM models with longer range interactions. However, even in these cases, $\mathfrak{g}(\mathcal{H})$ is significantly smaller than $|\mathfrak{su}(2^n)|$, which is an improvement over the generic case studied in Ref. [13].

Cartan Decomposition — Working with $\mathfrak{g}(\mathcal{H})$ instead of the full $\mathfrak{su}(2^n)$, we are left with needing to determine the parameters κ_i in Eq. (2). The Cartan decomposition and related methods in Ref. 13 and 17 provide the necessary tools to do so. We briefly review the Cartan decomposition and the "KHK theorem".

Definition 1 *Consider a compact semi-simple Lie subgroup $\boldsymbol{G} \subset SU(2^n)$, which has a corresponding Lie subalgebra $\mathfrak{g} \subset \mathfrak{su}(2^n)$. A **Cartan decomposition** on $\mathfrak{g}$ is defined as an orthogonal split $\mathfrak{g} = \mathfrak{k} \oplus \mathfrak{m}$ satisfying*

$$[\mathfrak{k}, \mathfrak{k}] \subset \mathfrak{k}, \qquad [\mathfrak{m}, \mathfrak{m}] \subset \mathfrak{k}, \qquad [\mathfrak{k}, \mathfrak{m}] = \mathfrak{m}, \quad (3)$$

*and denoted by $(\mathfrak{g}, \mathfrak{k})$. The **Cartan subalgebra** of this decomposition is defined as one of the maximal Abelian subalgebras of $\mathfrak{m}$ (and is denoted by $\mathfrak{h}$).*

In practice, the Lie subalgebra is partitioned by an involution. A Cartan involution is a Lie algebra homomorphism taking $\theta : \mathfrak{g} \to \mathfrak{g}$, which satisfies $\theta(\theta(g)) = g$ for any $g \in \mathfrak{g}$, preserves all commutators, and discriminates between $\mathfrak{k}$ and $\mathfrak{m}$ by $\theta(\mathfrak{k}) = \mathfrak{k}$ and $\theta(\mathfrak{m}) = -\mathfrak{m}$.

A consequence of Cartan decomposition, which we will utilize to synthesize Hamiltonian evolution unitaries, is the following theorem:

Theorem 1 *Given a Cartan decomposition $\mathfrak{g} = \mathfrak{k} \oplus \mathfrak{m}$, for any element $m \in \mathfrak{m}$ there exists a $K \in e^{\mathfrak{k}}$ and an $h \in \mathfrak{h}$, such that*

$$m = KhK^\dagger. \quad (4)$$

We can now describe the **second step of our algorithm:** Find a Cartan decomposition of $\mathfrak{g}(\mathcal{H})$ such that $\mathcal{H} \in \mathfrak{m}$. A direct application of Theorem 1 with $\mathcal{H} = KhK^\dagger$ then leads to the desired unitary for time-evolution

$$U(t) = e^{-i\mathcal{H}t} = Ke^{-iht}K^\dagger. \quad (5)$$

For the models discussed in Fig. 1, this step is achieved by simply using the involution $\theta(g) = -g^T$.

Note that the simulation time t in Eq. (5) enters as an independent parameter, and does not alter the structure of K or h. This means that new parameters do not need to be found for different simulation times (although this situation may change for time-dependent Hamiltonians).
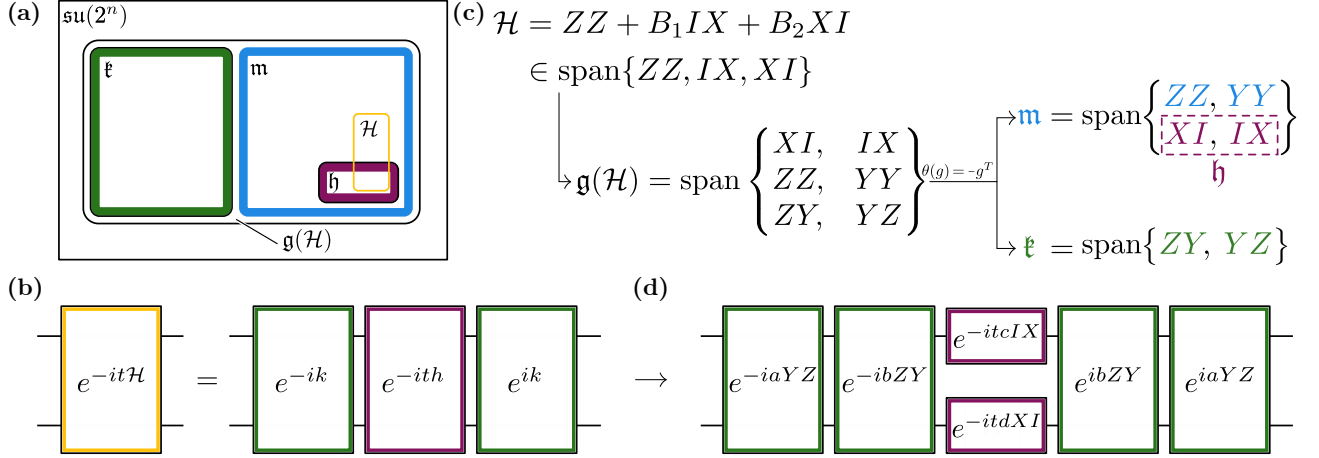
FIG. 2. (a) Schematic relationship of the Hamiltonian algebra $\mathfrak{g}(\mathcal{H})$ and its partitioning into a subalgebra $\mathfrak{k}$, its compliment $\mathfrak{m}$, and the Cartan subalgebra $\mathfrak{h}$. (b) KHK decomposition (Theorem 1) applied to a time evolution operator generated by an element of $\mathfrak{m}$. (c) Hamiltonian algebra $\mathfrak{g}(\mathcal{H})$ for the 2 site TFIM and the Cartan decomposition generated by the involution $\theta(\mathfrak{g}) = -\mathfrak{g}^T$. Here we list the bases that span $\mathfrak{g}(\mathcal{H})$ and its Cartan decomposition. (d) Decomposed time evolution for the 2-site TFIM model.

Determining Parameters — Following Ref. 17, K in Eq. (5) is determined by finding a *local* minimum of

$$f(K) = \langle KvK^\dagger, \mathcal{H}\rangle. \tag{6}$$

Here, $\langle .,.\rangle$ denotes the Killing form (i.e. the inner product on Pauli strings), and $v \in \mathfrak{h}$ is an element whose exponential map is dense in $e^{i\mathfrak{h}}$; *e.g.*, $v = \sum_i \gamma^i h_i$ where the h_i elements form a basis for $\mathfrak{h}$, and γ is an arbitrary transcendental number. Given any *local extremum* K_0 of $f(K)$, the relationship $K_0^\dagger \mathcal{H} K_0 = h \in \mathfrak{h}$ holds [17], which determines h and thus completes the decomposition.

There is a choice in how to represent the group element K. While Refs. 13 and 17 use $K = \exp(i\sum_i \alpha_i k_i)$, we express it as a factorized product similar to the full unitary

$$K = \prod_i e^{ia_i k_i}, \tag{7}$$

where k_i is an element of the Pauli string basis for $\mathfrak{k}$. Note that these two forms are equivalent due to the Baker-Campbell-Hausdorff theorem and the fact that $\mathfrak{k}$ is closed under commutation. Using the representation of K as in Eq. (7) has three benefits. First, the gradient of Eq. (6) can be obtained analytically; second, this allows us to apply K on v exactly (see supplementary material); and third, since a circuit implementation for individual Pauli strings is known [18, 19], we avoid the need for further decomposition of K.

We now reach the **third step of our algorithm:** Minimize Eq. (6) over the parameters a_i in K in Eq. (7) to find $K \in e^{\mathfrak{k}}$. In this work, we use a standard BFGS optimization routine. As detailed in the supplementary material, calculating Eq. (6) and its gradient from Eq. (7) require $\mathcal{O}(|\mathfrak{k}||\mathfrak{m}|)$ and $\mathcal{O}(|\mathfrak{k}|^2|\mathfrak{m}|)$ operations, respectively. For models where $|\mathfrak{g}(\mathcal{H})|$ is quadratic in the number of spins, these become $\mathcal{O}(n^4)$ and $\mathcal{O}(n^6)$.

Fig. 2 is a schematic illustration of the algorithm. Panel (a) shows the relationships between $\mathfrak{su}(2^n)$, the Hamiltonian $\mathcal{H}$, the Hamiltonian algebra $\mathfrak{g}(\mathcal{H})$, and its Cartan decomposition. Panel (b) shows the resulting factorization of the time-evolution operator. Panels (c) and (d) demonstrate steps one and two of our algorithm for a simple two-site Ising model. In this case, the Hamiltonian terms $\{ZZ, IX, XI\}$ generate a six dimensional Hamiltonian algebra $\mathfrak{g}(\mathcal{H})$, which is partitioned into $\mathfrak{k}$ and $\mathfrak{m}$ via the involution θ. There are two maximal Abelian subalgebras $\mathfrak{h}$ of $\mathfrak{m}$, namely span$\{ZZ, YY\}$ and span$\{XI, IX\}$; we choose the latter without loss of generality. The resulting factored time-evolution operator is shown in panel (d). This factorization is clearly suboptimal for the Hamiltonian evolution unitary in $SU(4)$, where a minimal 3-CNOT circuit is known [12]; however, our decomposition algorithm is applicable to any system size.

Application — To demonstrate the flexibility of our method, we synthesize time-evolution unitaries for a 10-site XY spin chain with open boundary conditions in the presence of a normally distributed, random, transverse field Z with mean zero and variance σ^2. The Hamiltonian for this model is

$$\mathcal{H} = \sum_{i=1}^{n-1}(X_i X_{i+1} + Y_i Y_{i+1}) + \sum_{i=1}^{n} b_i Z_i, \tag{8}$$

where $n = 10$ is the number of qubits and the b_i coefficients are the random variables; we use standard notation for the Pauli spin matrices. We consider a single spin-flip initial state $|\psi\rangle = |\downarrow\uparrow\uparrow\uparrow\uparrow\uparrow\uparrow\uparrow\uparrow\uparrow\rangle$. In the absence of the random magnetic field, this excitation diffuses throughout the system. By increasing the random magnetic field strength, the excitation is prevented from diffusing by the Anderson localization mechanism [20]. In one dimension, it has been shown that any p-th moment of the
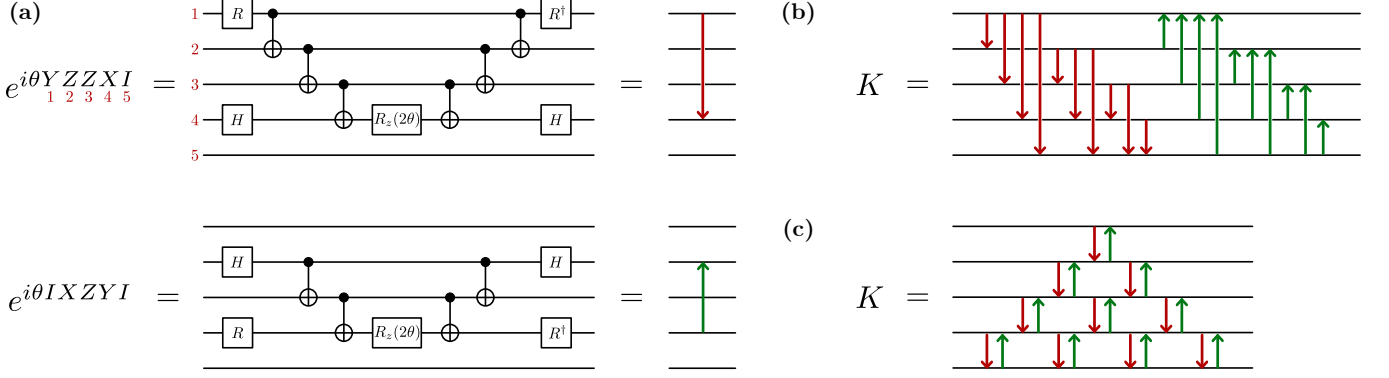
FIG. 3. (a) Circuit implementation of the given exponentials of Pauli strings, and the compact arrow notation. The R gate shown here is $R_x(\pi/2)$. (b/c) Unoptimized/optimized circuit for K in an $n = 5$ site TFXY model (this system size is chosen for illustrative purposes). The circuits have $\mathcal{O}(n^3)$ and $\mathcal{O}(n^2)$ CNOT gates, respectively.

displacement of the excitation has a time independent upper bound [21] $\langle |\hat{N}|^p \rangle < C_p$, where the position operator for the excitation is $\hat{N} = \sum_{r=1}^{n}(r-1)\frac{1-Z_r}{2}$.

We perform steps one and two of our algorithm. The Cartan decomposition and subalgebra for this model are

$$\mathfrak{k} = \text{span}\{\widehat{X_i Y}_j, \widehat{Y_i X}_j \,|\, i, j = 1, 2, .., n, \, i < j\},$$
$$\mathfrak{m} = \text{span}\{Z_j, \widehat{X_i X}_j, \widehat{Y_i Y}_j \,|\, i, j = 1, 2, .., n, \, i < j\}, \quad (9)$$
$$\mathfrak{h} = \text{span}\{Z_i \,|\, i = 1, 2, .., n\},$$

with dimensions $|\mathfrak{k}| = n(n-1)$, $|\mathfrak{m}| = n^2$ and $|\mathfrak{h}| = n$, and where the shorthand notation is defined to be

$$\widehat{A_i B}_j = A_i Z_{i+1} Z_{i+2} ... Z_{j-1} B_j. \quad (10)$$

We then perform step three of our algorithm and find the parameters minimizing Eq. (6).

In our resulting decomposition, the basis elements of $\mathfrak{k}$ are Pauli strings of Z that begin (end) with X and end (begin) with Y. Using (7) generates the circuit shown in Fig. 3(b), which has $2n(n^2 - 1)/3$ CNOT gates. As illustrated in Fig. 3(c), this circuit can be simplified to another circuit with $n(n-1)$ CNOT gates (see supplementary material for details).

For $n = 10$, the algorithm yields a circuit for $U(t)$ with 1320 CNOTs, which may be reduced via the optimization discussed above to 180 CNOTs. We compare the results of simulations conducted via our algorithm to Trotter evolution with a fixed number of CNOTs, varying the time step.

We used Trotter circuit depths equal to the optimized circuit (10 steps/180 CNOTS) and the un-optimized circuit (74 steps/1332 CNOTS).

Fig. 4 shows $N = \sqrt{\langle \hat{N}^2 \rangle}$, the RMS position of the single-spin excitation for various values of σ, as simulated with our algorithm and with Trotter time evolution. We renormalized the Hamiltonian for each standard deviation of the transverse field; i.e., $\mathcal{H} \rightarrow \frac{\mathcal{H}}{\sqrt{\text{tr}(\mathcal{H}^2)}}$ to eliminate any norm dependence of the time evolution. As

expected, the Trotter evolution diverges from the exact result after some time τ, which occurs later if there are more Trotter steps. τ depends on the standard deviation of disorder σ in the magnetic field; the results improve with increasing randomness because this decreases the relative diffusion probability for the excitation to hop to another site. Nevertheless, for any value of σ and any number of steps, the Trotter evolution eventually diverges from the exact result.

On the other hand, the result from the Cartan decomposition is indistinguishable from the exact solution.
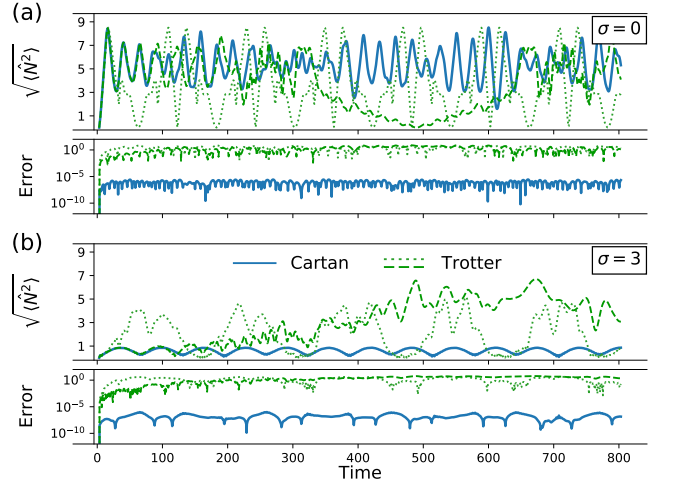
FIG. 4. Displacement of the spin excitation $N = \sqrt{\langle \hat{N}^2 \rangle}$ and its absolute difference from the exact result $|N - N_{\text{exact}}|$ in the TFXY model with a random Z field, for standard deviation $\sigma = 0$ in panel (a) and $\sigma = 3$ in panel (b). The excitation becomes trapped around its original position as the standard deviation of the magnetic field increases. The localization is captured to within a small constant error by our Cartan algorithm (solid curves). The error in the Trotterized spin displacement, which used 180 (dotted) and 1332 (dashed) CNOTs respectively, is larger by orders of magnitude.

We show the error (absolute deviation from the exact result) for the two methods in Fig. 4. Except for the earliest times, there are 4-6 orders of magnitude less error for the Cartan decomposition approach compared to the Trotter-based approach. Moreover, the error of the Cartan-based method does not increase with simulation time, which shows the suitability of this constant-depth circuit for long-time simulations. Note that the non-zero error for the Cartan-based algorithm stems from the non-zero gradient tolerance used in the optimization step of the algorithm, which was chosen to be 10^{-6} to obtain the data in Fig. 4.

Discussion. — We have introduced an efficient algorithm based on the Cartan decomposition for synthesizing unitaries which are generated by exponentiating an underlying Hamiltonian algebra. It has several benefits over previous methods, notably the analytic calculation of the cost function and its derivatives, immediate circuit construction, and only needing a single optimization for any time.

Our algorithm finds polynomial growth of the Hamiltonian algebra dimension for the TFIM and XY models. This can be traced back to a mapping from the spin representation to a non-interacting (free) fermionic model. In this sense, the Hamiltonian algebra reveals the existence of such a map. Our approach is complementary to a recent approach relying on evaluating graph invariants [15], and is simple to execute and thus determine if a map to a free fermion model exists. From this perspective, it is also clear why the Heisenberg model and models with long-range interactions have Hamiltonian algebras that do not scale polynomially; a Jordan-Wigner transformation maps these models onto *interacting* fermionic models.

While we have illustrated an exact version of our algorithm for simple toy problems, we expect it to be useful for problems which are significantly more complex. A generalization to the unitary coupled cluster formalism is direct and we will detail this application area in a future work. Another approach that can build upon Cartan decomposition is the use of symmetries and other problem structure, which are naturally expressed in this language. Interestingly, preliminary findings indicate that imposing symmetry complicates circuit construction while it reduces the dimension of the Hamiltonian algebra; this interplay between physical symmetry and algebraic analysis for quantum circuits merits future analysis. Finally, all our results so far have been exact; it will be interesting to examine approximate versions of our algorithm and understand the speedups and how they compare to conventional Hamiltonian evolution synthesis techniques.

ACKNOWLEDGMENTS

[1] B. Bauer, S. Bravyi, M. Motta, and G. Kin-Lic Chan, Chemical Reviews **120**, 12685 (2020).

[2] L. Bassman, M. Urbanek, M. Metcalf, J. Carter, A. F. Kemper, and W. de Jong, Simulating quantum materials with digital quantum computers (2021), arXiv:2101.08836 [quant-ph].

[3] S. Lloyd, Science **273**, 1073 (1996).

[4] J. Haah, M. B. Hastings, R. Kothari, and G. H. Low, SIAM Journal on Computing , FOCS18 (2021).

[5] A. M. Childs, Y. Su, M. C. Tran, N. Wiebe, and S. Zhu, Physical Review X **11** (2021).

[6] D. W. Berry, A. M. Childs, R. Cleve, R. Kothari, and R. D. Somma, Physical Review Letters **114**, 090502 (2015).

[7] G. H. Low and I. L. Chuang, Physical Review Letters **118**, 010501 (2017).

[8] G. H. Low and N. Wiebe, arXiv:1805.00675 (2018).

[9] A. Kalev and I. Hen, arXiv:2006.02539 (2020).

[10] M. C. Tran, Y. Su, D. Carney, and J. M. Taylor, PRX Quantum **2**, 010323 (2021).

[11] B. Şahinoğlu and R. D. Somma, arXiv:2006.02660 (2020).

[12] G. Vidal and C. M. Dawson, Physical Review A **69**, 010301 (2004).

[13] N. Khaneja and S. J. Glaser, Chemical Physics **267**, 11 (2001).

[14] B. Drury and P. Love, Journal of Physics A: Mathematical and Theoretical **41**, 395305 (2008).

[15] A. Chapman and S. T. Flammia, Quantum **4**, 278 (2020).

[16] Within the context of control theory, the Hamiltonian algebra is also referred to as the dynamical algebra: D. d'Alessandro, *Introduction to quantum control and dynamics* (CRC press, 2007).

[17] H. N. S. Earp and J. K. Pachos, Journal of Mathematical Physics **46**, 082108 (2005), https://doi.org/10.1063/1.2008210.

[18] J. D. Whitfield, J. Biamonte, and A. Aspuru-Guzik, Molecular Physics **109**, 735 (2011).

[19] A. Jayashankar, A. M. Babu, H. K. Ng, and P. Mandayam, Phys. Rev. A **101**, 042307 (2020).

[20] P. W. Anderson, Phys. Rev. **109**, 1492 (1958).

[21] V. Bucaj, arXiv:1608.01379 (2016).

[22] M. Dagli, D. D'Alessandro, and J. Smith, Journal of Physics A Mathematical and Theoretical **41** (2007).

Appendix A: Hamiltonian Algebras of Certain Models

1. XY Model

For the 1-D nearest neighbour XY model with open boundary conditions and arbitrary interaction coefficients,

$$\mathcal{H} = \sum_{i=1}^{n-1}(a_i X_i X_{i+1} + b_i Y_i Y_{i+1}), \tag{A1}$$

and the Hamiltonian algebra is found to be

$$\mathfrak{g}(\text{XY}) = \text{span}\{\widehat{X_i X}_{i+a}, \widehat{Y_i Y}_{i+a}, \widehat{X_i Y}_{i+b}, \widehat{Y_i X}_{i+b} \big| a \text{ odd}, b \text{ even}, 1 \le i, i+a, i+b \le n\}. \tag{A2}$$

The dimension of this algebra is calculated as $|\mathfrak{g}(\text{XY})| = 2\binom{n}{2} = n(n-1)$.

2. TFIM and TFXY Model

For the 1-D nearest neighbour transverse field XY model with open boundary conditions and free coefficients,

$$\mathcal{H} = \sum_{i=1}^{n-1}(a_i X_i X_{i+1} + b_i Y_i Y_{i+1}) + \sum_{i=1}^{n} c_i Z_i, \tag{A3}$$

the Hamiltonian algebra is found to be

$$\mathfrak{g}(\text{TFXY}) = \text{span}\{Z_j, \widehat{X_i X}_j, \widehat{Y_i Y}_j, \widehat{X_i Y}_j, \widehat{Y_i X}_j \big| 1 \le i, j \le n; \ i < j\}. \tag{A4}$$

The same algebra is found for transverse field Ising model, i.e. the $b_i = 0$ case for the Hamiltonian given in (A3). The dimension of this algebra is $|\mathfrak{g}(\text{TFXY})| = n + 4\binom{n}{2} = n(2n-1)$.

3. Heisenberg Model

For the 1-D nearest neighbour Heisenberg model with open boundary conditions and free coefficients,

$$\mathcal{H} = \sum_{i=1}^{n-1}(a_i X_i X_{i+1} + b_i Y_i Y_{i+1} + c_i Z_i Z_{i+1}), \tag{A5}$$

the Hamiltonian algebra is found to be

$$\mathfrak{g}(\text{Heisenberg}) = \text{span}\Big(\{\text{Pauli strings with } a \text{ many } X, b \text{ many } Y, c \text{ many } Z \big| a+b, a+c, b+c \text{ even}, a,b,c \ge 1\}$$
$$\setminus \{XXX...X, YYY...Y, ZZZ...Z\}\Big) \tag{A6}$$

All basis elements in this algebra commute with $XXX...X$, $YYY...Y$, and therefore also commute with $ZZZ...Z$. Any other Pauli string apart from the ones in algebra does not commute either with $XXX...X$ or $YYY...Y$.

In order to determine the dimension of $\mathfrak{g}(\text{Heisenberg})$, let us decompose $\mathfrak{su}(2^n) = \mathfrak{k} \oplus \mathfrak{m}$ with $\theta(g) = XXX...X \, g \, XXX...X$. Then $\mathfrak{k}$ is the subalgebra of $\mathfrak{su}(2^n)$ consisting of all the elements in $\mathfrak{su}(2^n)$ that commute with $XXX...X$. This decomposition of $\mathfrak{su}(2^n)$ is type A III, and resulting $\mathfrak{k}$ is isomorphic to $\mathfrak{k} \cong \mathfrak{su}(2^{n-1}) \oplus \mathfrak{su}(2^{n-1}) \oplus \mathfrak{u}(1)$ [14, 22]. To have all the elements that commute both with $XXX...X$ and $YYY...Y$, let us further decompose $\mathfrak{k}$ into $\mathfrak{k} = \mathfrak{k}' \oplus \mathfrak{m}'$ with the involution $\theta'(g) = YYY...Y \, g \, YYY...Y$. Therefore we have

$$\mathfrak{k}' = \text{span}\{\text{Pauli strings with } a \text{ many } X, b \text{ many } Y, c \text{ many } Z \big| a+b, a+c, b+c \text{ even}, a,b,c \ge 1\}. \tag{A7}$$

This decomposition does not affect $\mathfrak{u}(1)$ component of $\mathfrak{k}$. It only affects $\mathfrak{su}(2^{n-1})$ pieces separately, and leads to $\mathfrak{k}' \cong (\mathfrak{su}(2^{n-2}) \oplus \mathfrak{su}(2^{n-2}) \oplus \mathfrak{u}(1)) \oplus (\mathfrak{su}(2^{n-2}) \oplus \mathfrak{su}(2^{n-2}) \oplus \mathfrak{u}(1)) \oplus \mathfrak{u}(1)$. Therefore the dimension of $\mathfrak{k}'$ is $|\mathfrak{k}'| = 4|\mathfrak{su}(2^{n-2})| + 3 = 4^{n-1} - 1$.

The difference between the basis of $\mathfrak{k}'$ and $\mathfrak{g}(\text{Heisenberg})$ are the elements $XXX...X$, $YYY...Y$, and $ZZZ...Z$. Therefore the dimension of the Heisenberg Hamiltonian algebra can be calculated as $|\mathfrak{g}(\text{Heisenberg})| = |\mathfrak{k}'| - 3 = 4^{n-1} - 4$.

Appendix B: Involution for Certain Models

Pauli matrices satisfy $X^T = X$, $Y^T = -Y$, $Z^T = Z$. Using $(A \otimes B)^T = A^T \otimes B^T$, one finds that Pauli strings with an even number of Y matrices satisfy $\sigma^T = \sigma$, while the ones with an odd number of Y matrices satisfy $\sigma^T = -\sigma$. Therefore, for any Lie subalgera $\mathfrak{g} \subseteq \mathfrak{su}(2^n)$ using the involution $\theta(g) = -g^T$ which preserves commutation relations i.e. for any $a, b \in \mathfrak{g}$ we have $\theta([a,b]) = [\theta(a), \theta(b)]$, leads to a Cartan decomposition via $\theta(\mathfrak{k}) = \mathfrak{k}$, $\theta(\mathfrak{m}) = -\mathfrak{m}$ as

$$\begin{aligned} \mathfrak{k} &= \mathrm{span}\{\text{Pauli strings} \in \mathfrak{g} \text{ with odd } Y \text{ matrices}\}, \\ \mathfrak{m} &= \mathrm{span}\{\text{Pauli strings} \in \mathfrak{g} \text{ with even } Y \text{ matrices}\}. \end{aligned} \tag{B1}$$

The XY, transverse field XY, transverse field Ising and Heisenberg models have Hamiltonians consisting only of Pauli strings that have either 0 or 2 Y matrices, therefore satisfy $\theta(\mathcal{H}) = -\mathcal{H}^T = -\mathcal{H}$, which makes $\theta(g) = -g^T$ a suitable involution to apply Theorem 1 to these models.

Appendix C: 2 site TFIM Parameter Fit

As given in Fig. 2, the 2 site transverse field Ising model, $\mathcal{H} = ZZ + B_1 IX + B_2 XI$, has the following Hamiltonian algebra

$$\mathfrak{g}(\mathcal{H}) = \mathrm{span}\{XI, IX, ZZ, YY, YZ, ZY\}, \tag{C1}$$

and the following Cartan decomposition and Cartan subalgebra are used

$$\begin{aligned} \mathfrak{k} &= \mathrm{span}\{YZ, ZY\}, \\ \mathfrak{m} &= \mathrm{span}\{XI, IX, ZZ, YY\}, \\ \mathfrak{h} &= \mathrm{span}\{XI, IX\}. \end{aligned} \tag{C2}$$

By defining $v = IX + \gamma XI$, with γ an arbitrary transcendental constant, and $K = e^{iaYZ}e^{ibZY}$, the cost function (6) can be calculated as

$$\begin{aligned} f(a, b) &= \mathrm{tr}\left(e^{iaYZ}e^{ibZY}(IX + \gamma XI)e^{-ibZY}e^{-iaYZ}\mathcal{H}\right) \\ &= (B_1 + \gamma B_2)\cos 2a \cos 2b - (B_2 + \gamma B_1)\sin 2a \sin 2b + \cos 2a \sin 2b + \gamma \sin 2a \cos 2b. \end{aligned} \tag{C3}$$

To find a local extremum, we set $\partial f / \partial a = \partial f / \partial b = 0$, which yields

$$\begin{aligned} \tan(2a + 2b) &= \frac{1}{B_1 + B_2}, \\ \tan(2a - 2b) &= \frac{1}{B_2 - B_1}, \end{aligned} \tag{C4}$$

and are solved by

$$\begin{aligned} a &= \frac{1}{4}\arctan\left(\frac{1}{B_1 + B_2}\right) - \frac{1}{4}\arctan\left(\frac{1}{B_1 - B_2}\right), \\ b &= \frac{1}{4}\arctan\left(\frac{1}{B_1 + B_2}\right) + \frac{1}{4}\arctan\left(\frac{1}{B_1 - B_2}\right). \end{aligned} \tag{C5}$$

Plugging this in $K^\dagger \mathcal{H} K$, one finds

$$\begin{aligned} K^\dagger \mathcal{H} K &= e^{-ibZY}e^{-iaYZ}\mathcal{H}e^{iaYZ}e^{ibZY} \\ &= IX\left(\frac{(B_1 + B_2)^2 - 1}{2\sqrt{1 + (B_1 + B_2)^2}} - \frac{(B_1 - B_2)^2 - 1}{2\sqrt{1 + (B_1 - B_2)^2}}\right) \\ &\quad + XI\left(\frac{(B_1 + B_2)^2 - 1}{2\sqrt{1 + (B_1 + B_2)^2}} + \frac{(B_1 - B_2)^2 - 1}{2\sqrt{1 + (B_1 - B_2)^2}}\right) \\ &= c\,IX + d\,XI \in \mathfrak{h}. \end{aligned} \tag{C6}$$

With this, we have $\mathcal{H} = K(cIX + dXI)K^\dagger$, which is the desired relationship.

Appendix D: Time Complexity for Parameter Optimization

1. Cost function evaluation

To perform the optimization, we need to calculate $f(K) = \langle KvK^{\dagger}, \mathcal{H} \rangle$ [17] where $\mathcal{H} \in \mathfrak{m}$, $K \in e^{\mathfrak{k}}$ and v is an element in $\mathfrak{h}$ whose exponential map is dense in $e^{i\mathfrak{h}}$. In this work, we use $v = \sum_i \gamma^i h_i$ where γ is a transcendental number and the h_i form a basis for $\mathfrak{h}$, and represent K with the following product of exponentials

$$K = \prod_i e^{i\theta_i k_i}, \tag{D1}$$

where k_i form a basis for $\mathfrak{k}$. Using the fact that Killing form $\langle A, B \rangle$ in $\mathfrak{su}(2^n)$ is proportional to $\mathrm{tr}(AB)$ where tr is the matrix trace, we find

$$f(K) = \mathrm{tr} \Big(\prod_{i\uparrow} e^{i\theta_i k_i} \, v \prod_{i\downarrow} e^{-i\theta_i k_i} \, \mathcal{H} \Big), \tag{D2}$$

where $\uparrow$ ($\downarrow$) under the product means multiplication in an increasing (decreasing) order for i. Efficient calculation of this product is non-trivial because the products of these exponentials generally will not be in $\mathfrak{g}$, and thus may generate an arbitrary matrix in $\mathrm{GL}(2^n)$ and therefore require an exponential amount of calculation. One fact that can be used is that if $K \in e^{\mathfrak{k}}$ and $m \in \mathfrak{m}$, then we have $KmK^{\dagger} \in \mathfrak{m}$. Thus, if each exponential on both sides of v in (D2) is applied on v, one from each side at the same time (a similarity transformation), the result will always be in $\mathfrak{m}$. To apply the exponentials of k_i, one can take advantage of the fact that k_i are Pauli strings, therefore $k_i^2 = I$ and

$$e^{i\theta_i k_i} = \cos\theta_i \, I + i\sin\theta_i \, k_i. \tag{D3}$$

This allows us to apply one similarity transformation on one term in v via constant amount of calculations only requires a constant amount of calculations. After applying all exponentials to v,

$$f(K) = \mathrm{tr} \Big(m_0 \mathcal{H} \Big) \tag{D4}$$

is obtained, where

$$m_0 = \prod_{i\uparrow} e^{i\theta_i k_i} \, v \prod_{i\downarrow} e^{-i\theta_i k_i} \in \mathfrak{m}. \tag{D5}$$

Up to this point, in the worst case only $\mathcal{O}(|\mathfrak{k}||\mathfrak{m}|)$ many operations are performed. $|\mathfrak{k}|$-many exponentials are applied to an element of $\mathfrak{m}$, which has at most $|\mathfrak{m}|$ many Pauli terms. Multiplying m_0 and $\mathcal{H}$ requires $\mathcal{O}(|\mathfrak{m}|)$ many calculations and can be neglected in the $|\mathfrak{k}| \gg 1$ limit corresponding to large system size limit, which leads to $\mathcal{O}(|\mathfrak{k}||\mathfrak{m}|)$ time complexity to calculate $f(K)$.

2. Gradient evaluation

The gradient of K given in (D1) can be expressed as

$$\frac{\partial K}{\partial \theta_j} = \prod_{i<j,\uparrow} e^{i\theta_i k_i} ik_j \prod_{i\geq j,\uparrow} e^{i\theta_i k_i}, \tag{D6}$$

leading to the analytical expression for the gradient of the function (D2):

$$\begin{aligned}
\frac{\partial f(K)}{\partial \theta_j} = {} & \mathrm{tr} \Big(\prod_{i<j,\uparrow} e^{i\theta_i k_i} ik_j \prod_{i\geq j,\uparrow} e^{i\theta_i k_i} \, v \prod_{i\downarrow} e^{-i\theta_i k_i} \, \mathcal{H} \Big) \\
& + \mathrm{tr} \Big(\prod_{i\uparrow} e^{i\theta_i k_i} \, v \prod_{i\geq j,\downarrow} e^{i\theta_i k_i} (-i)k_j \prod_{i<j,\downarrow} e^{-i\theta_i k_i} \, \mathcal{H} \Big).
\end{aligned} \tag{D7}$$

Using the cyclic property of trace $\text{tr}(AB) = \text{tr}(BA)$ leads to

$$\frac{\partial f(K)}{\partial \theta_j} = i\,\text{tr}\left(k_j \prod_{i \geq j,\uparrow} e^{i\theta_i k_i}\, v \prod_{i\downarrow} e^{-i\theta_i k_i}\, \mathcal{H} \prod_{i<j,\uparrow} e^{i\theta_i k_i}\right)$$
$$-i\,\text{tr}\left(\prod_{i<j,\downarrow} e^{-i\theta_i k_i}\, \mathcal{H} \prod_{i\uparrow} e^{i\theta_i k_i}\, v \prod_{i \geq j,\downarrow} e^{i\theta_i k_i}\, k_j\right) \tag{D8}$$

Applying the exponentials one by one from both sides of v and $\mathcal{H}$, we obtain

$$\frac{\partial f(K)}{\partial \theta_j} = i\,\text{tr}\left(k_j\, m_1\, e^{-i\theta_j k_j}\, m_2\right) - i\,\text{tr}\left(m_2\, e^{i\theta_j k_j}\, m_1\, k_j\right). \tag{D9}$$

where

$$m_1 = \prod_{i \geq j,\uparrow} e^{i\theta_i k_i}\, v \prod_{i \geq j\downarrow} e^{-i\theta_i k_i} \in \mathfrak{m}$$
$$m_2 = \prod_{i<j\downarrow} e^{-i\theta_i k_i}\, \mathcal{H} \prod_{i<j,\uparrow} e^{i\theta_i k_i} \in \mathfrak{m}. \tag{D10}$$

As in the calculation of $f(K)$, reaching that point costs $\mathcal{O}(|\mathfrak{k}||\mathfrak{m}|)$ amount of time and in the $|\mathfrak{k}| \gg 1$ limit corresponding to large system size limit, it is the most time consuming part compared to the last calculation of trace which takes $\mathcal{O}(|\mathfrak{m}|)$ time as above. However, this complexity is to obtain just one derivative. To calculate the full gradient, one has to perform this for all θ_j, and therefore the complexity of calculating the entire gradient is $\mathcal{O}(|\mathfrak{k}|^2|\mathfrak{m}|)$.

Appendix E: Circuit Optimization for TFXY Model

In this section, we outline several circuit optimizations which we apply to the free-fermionizable model discussed in the main text.

Consider an n-qubit circuit. We establish the following Lemma:

Lemma 1 *For any $i, j = 1, 2, ..., n-1$, $i < j$ and any $\alpha, \beta \in \mathbb{R}$, there exist $a, b, c \in \mathbb{R}$ such that*

$$e^{i\alpha\widehat{Y_iX}_j} e^{i\beta\widehat{Y_iX}_{j+1}} = e^{ia\widehat{Y_jX}_{j+1}} e^{ib\widehat{Y_iX}_j} e^{ic\widehat{Y_jX}_{j+1}} \tag{E1}$$

where the "hat" notation is defined in Eq. (10). The same is true for $X \leftrightarrow Y$.

To prove this, observe that the algebra generated by the exponents of the left hand side is a representation of $\mathfrak{su}(2)$:

$$[\widehat{Y_iX}_{j+1}, \widehat{Y_iX}_j] = 2i\,\widehat{Y_jX}_{j+1}$$
$$[\widehat{Y_jX}_{j+1}, \widehat{Y_iX}_{j+1}] = 2i\,\widehat{Y_iX}_j \tag{E2}$$
$$[\widehat{Y_iX}_j, \widehat{Y_jX}_{j+1}] = 2i\,\widehat{Y_iX}_{j+1}$$

Thus, (E1) is an Euler decomposition of a $\mathfrak{su}(2)$ spanned by the Pauli strings. The version with $X \leftrightarrow Y$ is also true for the same reason.

Using the arrow notation introduced in Fig. 3, a graphical representation of Lemma 1 can be given as
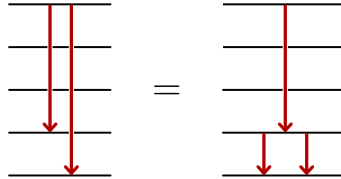
FIG. S1. Graphical representation of Lemma 1 for $i = 1, j = 4$.

Next, we apply this Lemma to an ordered product of exponentials as is used in Eqs. (D2) and (D6).

Theorem 2 *We define a "triangle" of size i as*

$$T_i(\vec{\alpha}) = \prod_{j=1}^{i} e^{i\alpha_j \widehat{Y_1 X}_j} \tag{E3}$$

and

$$Z_{p,q}(\vec{\alpha}) = \prod_{j=p}^{q} e^{i\alpha_j \widehat{Y_j X}_{j+1}} \tag{E4}$$

which will be denoted as "zig" if $p > q$ and "zag" if $p < q$. Then for $i \geq 3$, there exists a new set of parameters $\vec{a}, b, c \in \mathbb{R}$ such that

$$T_i(\vec{\alpha}) = e^{ib\widehat{Y_{j-1} X}_j} T_{i-1}(\vec{a}) e^{ic\widehat{Y_{j-1} X}_j} \tag{E5}$$

and this implies for a new set of parameters $\vec{\beta}, \vec{\theta} \in \mathbb{R}$, the "triangle" $T_i(\vec{\alpha})$ can be written as a "zigzag"

$$
\begin{aligned}
T_i(\vec{\alpha}) &= \prod_{j=i-1,\downarrow}^{1} e^{i\beta_j \widehat{Y_j X}_{j+1}} \prod_{j=1}^{i-1} e^{i\theta_j \widehat{Y_j X}_{j+1}} \\
&= Z_{i-1,1}(\vec{\beta}) Z_{2,i-1}(\vec{\theta}).
\end{aligned} \tag{E6}
$$

To prove this, we first observe that

$$
\begin{aligned}
T_i(\vec{\alpha}) &= \prod_{j=1}^{i} e^{i\alpha_j \widehat{Y_1 X}_j} \\
&= \left(\prod_{j=1}^{i-2} e^{i\alpha_j \widehat{Y_1 X}_j} \right) e^{i\alpha_{i-1} \widehat{Y_1 X}_{i-1}} e^{i\alpha_i \widehat{Y_1 X}_i}.
\end{aligned} \tag{E7}
$$

Using Lemma 1 on the last two exponentials, and renaming new parameters:

$$
\begin{aligned}
T_i(\vec{\alpha}) &= \left(\prod_{j=1}^{i-2} e^{ia_j \widehat{Y_1 X}_j} \right) e^{ib\widehat{Y_{i-1} X}_i} e^{ia_{i-1} \widehat{Y_1 X}_{i-1}} e^{ic\widehat{Y_{i-1} X}_i} \\
&= e^{ib\widehat{Y_{i-1} X}_i} \left(\prod_{j=1}^{i-2} e^{ia_j \widehat{Y_1 X}_j} \right) e^{ia_{i-1} \widehat{Y_1 X}_{i-1}} e^{ic\widehat{Y_{i-1} X}_i} \\
&= e^{ib\widehat{Y_{i-1} X}_i} \left(\prod_{j=1}^{i-1} e^{ia_j \widehat{Y_1 X}_j} \right) e^{ic\widehat{Y_{i-1} X}_i} \\
&= e^{ib\widehat{Y_{i-1} X}_i} T_{i-1}(\vec{a}) e^{ic\widehat{Y_{i-1} X}_i},
\end{aligned} \tag{E8}
$$

which is just equation (E5). Recursively iterating this a total of $i-1$ times, results in Eq. (E6). In the graphical representation, this recursion is easy to see as shown in Fig. S2.
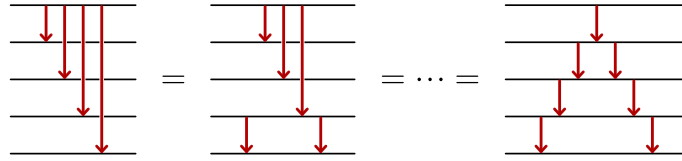
FIG. S2. Graphical representation of Theorem 2 for $i = 5$.

Considering the fact that the original circuit is a product of triangles, we now show that it can be written as a series of zigzags schematically depicted in Fig. S3. This greatly reduces the complexity of the circuit because the initial circuit given on the left has $\mathcal{O}(n^3)$ CNOT gates, whereas the simplified zigzag circuit has only $\mathcal{O}(n^2)$ CNOT gates. However, this circuit can be simplified further.
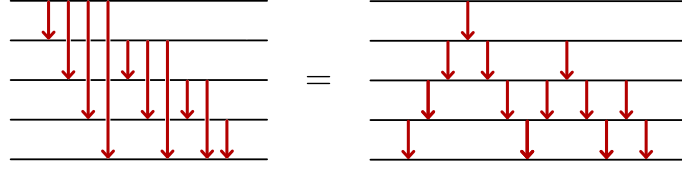
FIG. S3. First simplification of the initial circuit for K.

Lemma 2 *Any zigzag can be flipped into a "zagzig", i.e. for any $i \geq 2$ and any set of parameters $\alpha_j, \beta_j \in \mathbb{R}$, there exists $\vec{a}, \vec{b} \in \mathbb{R}$ such that*

$$Z_{i,1}(\vec{\alpha})Z_{2,i}(\vec{\beta}) = Z_{1,i}(\vec{a})Z_{i-1,1}(\vec{b}) \tag{E9}$$

The proof is by induction. The base case is for zigzags with size $i = 2$, because $\widehat{Y_2 X_3}, \widehat{Y_1 X_2}, \widehat{Y_1 X_3}$ forms a representation of $\mathfrak{su}(2)$ and it is established by using the Euler decomposition in the following two ways:

$$e^{ia\widehat{Y_1 X_2}}e^{ib\widehat{Y_2 X_3}}e^{ic\widehat{Y_1 X_2}} = e^{i\alpha\widehat{Y_2 X_3}}e^{i\beta\widehat{Y_1 X_2}}e^{i\theta\widehat{Y_2 X_3}}. \tag{E10}$$

This is precisely the $i = 2$ case of the lemma. Now we assume that it also holds for all zigzags up to size N. Then for $i = N + 1$, we have that

$$Z_{N+1,1}(\vec{\alpha})Z_{2,N+1}(\vec{\beta}) = Z_{N+1,3}(\vec{\alpha})\Big(e^{i\alpha_2\widehat{Y_2 X_3}}e^{i\alpha_1\widehat{Y_1 X_2}}e^{i\beta_2\widehat{Y_2 X_3}}\Big)Z_{3,N+1}(\vec{\beta}) \tag{E11}$$

The product in parentheses is our base case shown in Eq. (E10). Therefore, for some $a, b, c \in \mathbb{R}$, we have that

$$\begin{aligned}
Z_{N+1,1}(\vec{\alpha})Z_{2,N+1}(\vec{\beta}) &= Z_{N+1,3}(\vec{\alpha})\Big(e^{ia\widehat{Y_1 X_2}}e^{ib\widehat{Y_2 X_3}}e^{ic\widehat{Y_1 X_2}}\Big)Z_{3,N+1}(\vec{\beta}) \\
&= e^{ia\widehat{Y_1 X_2}}\Big(Z_{N+1,3}(\vec{\alpha})\ e^{ib\widehat{Y_2 X_3}}Z_{3,N+1}(\vec{\beta})\Big)e^{ic\widehat{Y_1 X_2}}.
\end{aligned} \tag{E12}$$

Note that the expression inside the parentheses on the last line is a zigzag with size N, that runs between sites 2 and $N + 1$. Therefore it can be flipped by the induction hypothesis. After renaming the parameters $a \to a_1$ and $c \to c_1$, we obtain

$$\begin{aligned}
Z_{N+1,1}(\vec{\alpha})Z_{2,N+1}(\vec{\beta}) &= e^{ia_1\widehat{Y_1 X_2}}\Big(Z_{2,N+1}(\vec{a})Z_{N,2}(\vec{b})\Big)e^{ic\widehat{Y_1 X_2}} \\
&= Z_{1,N+1}(\vec{a})Z_{N,1}(\vec{b}),
\end{aligned} \tag{E13}$$

which proves the induction step. This completes the proof of Lemma 2. A graphical representation is given in Fig. S4.
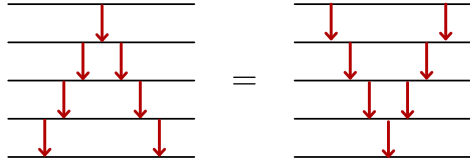
FIG. S4. Graphical representation of Lemma 2 for $i = 5$.

Theorem 3 *The zigzag circuit given for K can be simplified into a more compact multiplications of "zigs", i.e. for every $n \geq m + 1$, $\vec{\alpha}_i, \vec{\beta}_i \in \mathbb{R}$ there exist a set of $\vec{\theta}_i \in \mathbb{R}$, such that*

$$\prod_{i=m}^{n-1}\Big(Z_{n,i}(\vec{\alpha}_i)Z_{i+1,n}(\vec{\beta}_i)\Big) = \prod_{i=m}^{n} Z_{n,i}(\vec{\theta}_i). \tag{E14}$$

For convenience, the parameters will not be shown explicitly for this proof i.e. $Z_{n,m}(\vec{\alpha})$ will be written as $Z_{n,m}$, since the parameters are not determined explicitly in the argument. The proof is again by induction. The base case is for $n - m = 1$ since both sides become $Z_{m+1,m}Z_{m,m}$. Now, assume that the induction step holds for all $n - m$ up

to $n - m = N \geq 1$. We will next establish that it holds for $n - m = N + 1$. First, define $N' = N + m + 1$ and then regroup the product to obtain

$$\prod_{i=m}^{N'-1} \left(Z_{N',i} Z_{i+1,N'}\right) = Z_{N',m} \prod_{i=m+1}^{N'-1} \left(Z_{i,N'} Z_{N',i}\right) Z_{N',N'}. \tag{E15}$$

Since $N' > i$, $Z_{i,N'} Z_{N',i}$, the product of terms in the parenthesis can be rewritten as $Z_{i,N'} Z_{N'-1,i}$, yielding

$$= Z_{N',m} \prod_{i=m+1}^{N'-1} \left(Z_{i,N'} Z_{N'-1,i}\right) Z_{N',N'}. \tag{E16}$$

Using Lemma 2 for the expression in the product, we find that the product becomes

$$= Z_{N',m} \prod_{i=m+1}^{N'-1} \left(Z_{N',i} Z_{i+1,N'}\right) Z_{N',N'}$$

$$= Z_{N',m} \prod_{i=m+1}^{N'-1} \left(Z_{N',i} Z_{i,N'}\right). \tag{E17}$$

In the last step, we used the fact that the last term in the product in the middle is $Z_{N',N'}$ and therefore can be absorbed into the term after the product by redefining its coefficient in the exponent.

Note that the product term to the right is part of the induction hypothesis for $n - m = N$. Applying the induction hypothesis gives us

$$= Z_{N',m} \prod_{i=m+1}^{N'} \left(Z_{N',i}\right)$$

$$= \prod_{i=m}^{N'} \left(Z_{N',i}\right), \tag{E18}$$

which proves the induction step, and establishes the theorem. A graphical representation is given in Fig. S5.
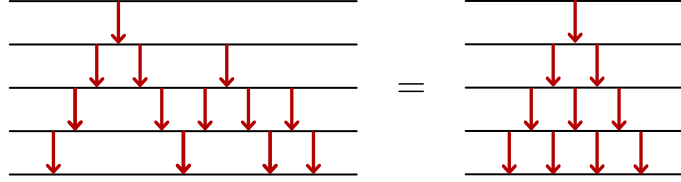
FIG. S5. Graphical representation of theorem 3 for $n = 4$ and $m = 1$.

Using these results, we find that the red part of the original K circuit, given in the left side of Fig. S3. can be rewritten as the circuit on right shown in Fig. S4. Considering that all the down red arrows commute with all the up green arrows, we can move greens through the reds and arrive at the simplification shown in Fig. S6.
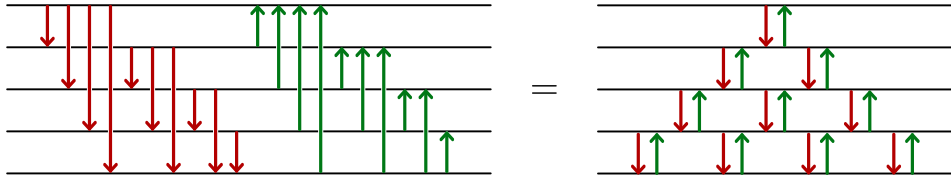
FIG. S6. Simplification of K circuit for Transverse Field XY model for 5 spins.

As shown in Fig. 3(a), an arrow with length a, $i.\ e.$, the circuit for $\exp(i\theta \widehat{X_i Y}_{i+a})$ (or the same circuit, but with $X \leftrightarrow Y$), has $2a$ CNOT gates in it. Therefore, the number of CNOT gates in the circuit on the left of Fig. S6 satisfies

$$\#\text{CNOTs for raw } K = (\text{red part}) + (\text{green part}) = 2\sum_{p=1}^{n-1}\sum_{q=1}^{p}(2q) = 2\sum_{p=1}^{n-1} p(p+1) = \frac{2n(n^2-1)}{3}. \tag{E19}$$

On the other hand, the optimized circuit for n spins consists pairs of length one red arrows followed by length one green arrows, that is $\exp(i\theta \widehat{Y_i X}_{i+1}) \exp(i\phi \widehat{X_i Y}_{i+1})$. A circuit for this pair requires only 2 CNOTs [12]. Therefore, the total CNOT count of the simplified circuit on the left of Fig. S6 is reduced to only the following:

$$\#\text{CNOTs for simplified } K = \sum_{p=1}^{n-1} (2p) = n(n-1). \tag{E20}$$

The full circuit consists of one factor of K, one factor of $\exp(-ith)$ and one factor of $K^\dagger$, as given in Fig. 2(b). Using the Cartan subalgebra given in (9), we see that $\exp(-ith)$ does not require any CNOT gates. Hence, the complete time-evolution circuit of $U(t) = K\exp(-ith)K^\dagger$ has twice as many CNOTs as the circuit for one K has. Therefore, the non-optimized circuit for time evolution has $4n(n^2-1)/3$ CNOTs, whereas the optimized one has only $2n(n-1)$ CNOTs.